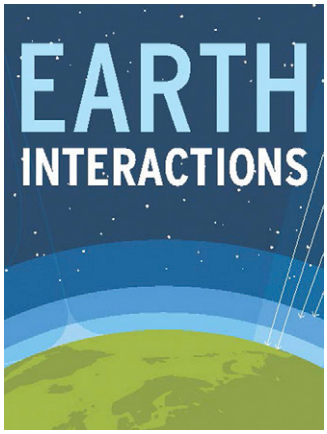

Passive Suppression of South African Rainfall by the Agulhas Current

Mark R. Jury*

University of Zululand, KwaDlangezwa, South Africa, and Physics Department, University of Puerto Rico Mayagüez, Mayagüez, Puerto Rico

Received 16 March 2015; in final form 14 August 2015

ABSTRACT: This study reconsiders the role of the Agulhas Current in South African climate variability. Here, the Agulhas Current is delimited by its anticyclonic looping flow and cluster analysis of detrended SST anomalies that lead to an area 28°–37°S, 18°–35°E, poleward of South Africa. Regression of detrended Agulhas SST with rainfall anomaly fields in the years 1950–2012 yields a surprising negative influence over the interior. In summer, the negative regression exhibits a northwest axis consistent with reduced cloud band activity. Positive influence is confined to the eastern escarpment in the September–November season when cutoff lows are prevalent. The overall negative influence of the Agulhas SST is confirmed by regression with the vegetation fraction and latent heat flux in the satellite era.

Mechanisms of South African rainfall suppression were investigated. The Agulhas SST index is positively related to the multivariate ENSO index at the 1–3-month lead time. Hence, warm years in the Agulhas Current follow Pacific El Niño. Composite ocean analysis shows enhanced westerly winds offshore and a westward extension of warm salty water from the

* Corresponding author address: Mark R. Jury, Physics Dept., University of Puerto Rico Mayagüez, P.O. Box 9000, Mayagüez, Puerto Rico, 00681.

E-mail address: mark.jury@upr.edu

DOI: 10.1175/EI-D-15-0017.1

anticyclonic south Indian Ocean gyre. Composite atmospheric analysis exhibits moist uplifted air over the Agulhas Current folding into an equatorward circulation that sinks over the interior plateau. Because Agulhas SST partially follows ENSO, its suppression of interior rainfall is concluded to be passive.

KEYWORDS: Atmosphere–ocean interaction; Boundary currents; ENSO

1. Introduction

The ocean stores heat and drives the Earth's water cycle, while integrating surface energy exchanges and providing memory of past fluxes to sustain atmospheric anomalies. Heat imbalances generate atmosphere and ocean circulations, which seek to minimize those gradients. Western boundary currents that transport warm tropical water poleward along the continental margins play a key role by contributing surplus energy to passing storms. Conversely, eastern boundary currents that advect cool upwelled water equatorward draw energy from the atmosphere and inhibit convection. There is only one place in the world where opposing boundary currents ''touch'': south of Africa.

Understanding South African climate variability is challenging because of the mixture of local and remote influences and the juxtaposition of moisture sources and sinks (Hulme et al. 1996). The Pacific El Niño–Southern Oscillation (ENSO) modulates the zonal atmospheric circulation over the southeast Atlantic (Mo and Paegle 2001). During the warm phase, westerlies bring dry air from the cool Benguela Current onto the South African Plateau. In the cold phase, easterlies transport humid air from the warm Agulhas Current (Mason and Jury 1997; Reason 2001). South Africa's economic output varies according to rainfall (Schulze et al. 1993; Jury 2002) contributed by northwest (NW)-oriented cloud bands in summer and cutoff lows in transition seasons (Harrison 1984; Barclay et al. 1993; Rouault et al. 2002; Hart et al. 2013). The moisture balance that enables crop production is subject to land–sea shifts in convective anomalies (Fauchereau et al. 2009).

The Agulhas Current that flows down the southeast flank of South Africa at $>1\,\mathrm{m\,s^{-1}}$ provides moisture to the atmospheric boundary layer via latent heat fluxes (Walker and Mey 1988; Walker 1990) (Figures 1a–c). The coastal climate owes a debt to the Agulhas Current (Jury et al. 1993), particularly under ridging high pressure conditions, when onshore flow gains thermodynamic energy (Jury et al. 1997) and rain falls over the narrow coastal belt of the eastern cape and KwaZulu-Natal. However, the relationship of NW cloud band rainfall over the interior plateau to sea surface temperature (SST) anomalies in the Agulhas Current remains obscure.

A hypothesis is explored that the Agulhas Current passively suppresses South African rainfall anomalies as it follows ENSO. The Agulhas Current is defined as the warm poleward boundary current and retroflection zone south of South Africa. Excluded in this definition are the inflow and outflow zones of the Agulhas Current linked with the vast ocean gyre circulations (Hermes et al. 2007). The paper outlines the data and methods utilized, followed by results on the mean state and sensitivity of South African rainfall anomalies to the Agulhas SST. Air–sea

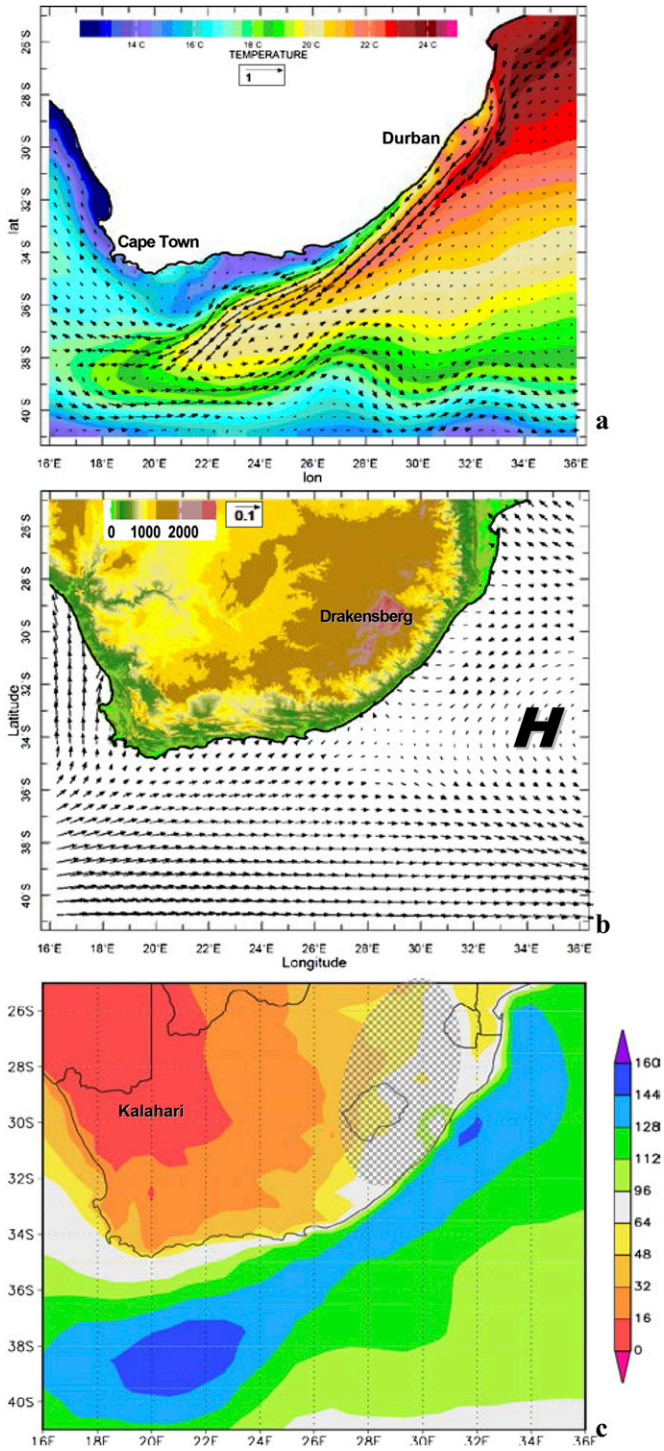

Figure 1. Climatological mean: (a) 1–100-m ocean currents and sea temperature, (b) marine wind stress (N m^{-2}) and South African topography, and (c) latent heat flux with $\sigma > 15$ W m^{-2} shaded; all from reanalysis averaged over the 1980–2012 period. The thermal high pressure ridge is identified in (b).

interactions emerge in composite analysis, and a concluding discussion highlights the key features.

2. Data and methods

This section describes the data and analysis techniques used to determine the climatic influence of the Agulhas Current. The domain considered is 25°–41°S, 16°–36°E (Figure 1a). This contains the whole of the Agulhas Current and all of South Africa except the Limpopo Valley bordering Zimbabwe. Past studies have defined the Agulhas Current as extending into the South Atlantic and Indian Oceans, whereas here it is limited to the zone south of South Africa where current velocities exceed 1 m s^{-1}. The time period for the analysis is from January 1950 to December 2012 for the 1° interpolated Hadley SST (Kennedy et al. 2011) and 0.5° Global Precipitation Climatology Center (GPCC), version 6, land rainfall (Schneider et al. 2014). These interpolated products are based on ship and station data, blended with satellite radiance information since 1981. The ship traffic and station network have remained dense and consistent over the study area and time period. The availability of satellite data corresponds with 1.8° atmosphere and 1.0° ocean reanalyses from the National Centers for Environmental Prediction (NCEP-2 and GODAS) (Derber and Rosati 1989; Kanamitsu et al. 2002; Behringer 2007; Huang et al. 2008). Terrestrial products include the 0.3° National Aeronautics and Space Administration (NASA) satellite vegetation fraction [normalized difference vegetation index (NDVI); Tucker et al. 2005] and 0.05° Climate Hazards Group Infrared Precipitation with Stations (CHIRPS), version 2, coastal rainfall (Funk et al. 2014) since 1981. The surface latent heat flux (LHF) is from the 0.6° gridded NASA Modern Era-Retrospective Analysis for Research and Applications (MERRA) reanalysis (Rienecker et al. 2011) and quantifies the evaporation rate via the bulk aerodynamic formula as a product of surface wind-induced turbulence and the vertical gradient of specific humidity. The MERRA LHF product has benefits over earlier reanalyses in representing local moisture sources and sinks (Jimenez et al. 2011; Roberts et al. 2012).

The climatological mean is calculated by averaging SST and related fields over the satellite era (1980+). Empirical orthogonal function analysis was used to find the thermal footprint of the Agulhas Current in Hadley SST fields over 25°–41°S, 16°–36°E in the period 1950–2012, after filtering the linear trend and annual cycle. The loading pattern maximum over the Agulhas Current contrasts with an offshore zone (Figure 2a). To avoid ambiguities from a dipole, an index is formulated by averaging SST anomalies over 28°–37°S, 18°–35°E from Durban to Cape Town. Subsequent statistical analyses make use of this index, after removal of the +0.004°C yr^{-1} trend that accounts for 11% of variance (Figure 2b). The SST index is regressed onto GPCC rainfall anomaly fields over South Africa continuously and in 3-month seasons for 1950–2012 and onto the satellite vegetation fraction for 1981–2006. Various other datasets and time periods are explored to confirm a stable result, and the regression is repeated for LHF. NCEP-2 and GODAS atmosphere and ocean circulation differences are studied for a group of contrasting warm and cool years, identified by ranking the detrended Agulhas SST index in the satellite era: warm—1983, 1992, 1993, 1999, 2000, and 2007—and cold—1981, 1982, 1988, 1990, 1995, and 1996. The successive-year pattern is related to natural

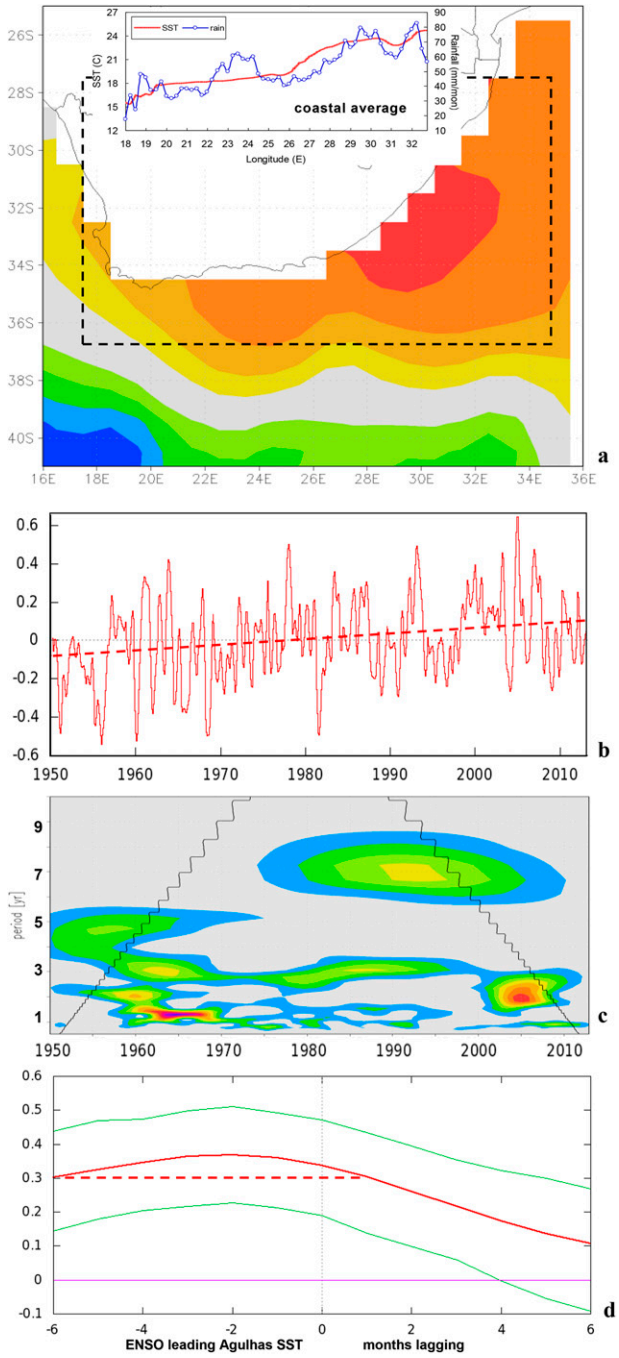

Figure 2. (a) Spatial loading pattern of the Agulhas mode calculated from continuous SST anomalies, contoured from −1 to +1 σ. (b) Agulhas SST index and its (c) wavelet spectral energy contoured >80% confidence with cone of validity. (d) Lag correlation of ENSO–MEI with detrended SST index, values above dashed line > 90% confidence. The inset in (a) is mean coastal rain vs mean SST; dashed box is the index area. The linear trend that is removed prior to statistical analysis is shown in (b).

persistence in the marine climate and to calendar years dividing the southern summer and ENSO influence. Warm minus cold composite fields are calculated for upper-ocean currents and salinity, surface winds, and latent heat fluxes and the meridional atmospheric circulation and humidity. The detrended Agulhas SST index is subjected to wavelet spectral analysis and lag correlation with a multitude of known climate indices such as the multivariate ENSO index (MEI) (Wolter and Timlin 2011). With ~28 degrees of freedom, correlation values $>|0.31|$ are deemed to be significant at 90% confidence. Statistical methods are similar to Nakamura (2012).

3. Results

3.1. Climatology

The ocean and atmosphere mean state over the Agulhas Current is illustrated in Figures 1a–c. This figure also serves to introduce the South African topography, dominated by a vast interior plateau at 1500 m and a narrow coastal margin. The Agulhas Current flows along the southeast coast, hugging the shelf east of 26°E (Figure 1a). The current spreads offshore and diffuses westward near Cape Town at 19°E. Much of the current turns eastward along 38°S around the edge of the anticyclonic south Indian Ocean gyre, which borders the warm part of the Agulhas SST signal. The prevailing surface winds (Figure 1b) are from the west in the offshore zone west of 26°E. Over the warm pool, mean winds are weak due to the cancellation of alternating seasonal circulations and the presence of a thermal high pressure ridge. Latent heat fluxes (Figure 1c) exceed 120 W m^{-2} over and just southeast of the Agulhas Current (Rouault et al. 2003). In the Kalahari Desert there is little evaporation. The standard deviation of LHF is largest (>15 W m^{-2}) over the Drakensberg escarpment between Lesotho and Swaziland. The mean map of MERRA latent heat flux emphasizes the close proximity of moisture sources and sinks. Coastal rainfall follows the mean coastal SST (inset Figure 2a) despite variations in orography, suggesting that much of the rainfall involves onshore flow from the Agulhas Current. The mean value slopes upward with longitude.

3.2. Agulhas SST variability

The SST cluster analysis (Figure 2a) yields an Agulhas mode with a spatial loading maximum extending from the southeast coast to 37°S and an opposing minimum along the southwestern edge of the domain outside the Agulhas Current. The loading maximum includes both warm and cold sectors, the former embedded in strong currents and the latter affected by Ekman transport over the continental shelf (cf. Figure 1). Despite the diverse factors, they fluctuate together. The temporal analysis (Figures 2b,c) reveals spikes near the annual cycle, although the SST index is filtered. The interpretation is a continual shifting of the annual cycle (Matano et al. 2002), particularly in the 1960s. Periodic fluctuations are noteworthy at 3 years in the 1960s and 1980s, 5 years in the 1950s, and 7 years from 1980 to 2005 (Figure 2c). The Agulhas SST fluctuates with Pacific ENSO as represented by the MEI correlation $> +0.35$ at lead times from 1 to 3 months (Figure 2d).

Underlying processes that emerge in the composite analysis below include an accelerated gyre circulation. Climate indices from the Indian and Atlantic Oceans and Southern Hemisphere all failed to show significant correlation with the Agulhas SST index.

3.3. South African climate influence

Regression of the detrended Agulhas SST index onto GPCC rainfall anomalies from 1950 to 2012 is mapped over South Africa in Figures 3a–e. The continuous data feature a surprising negative signal $< -10\,\mathrm{mm\,month^{-1}\,°C^{-1}}$ across the interior plateau. Rouault et al. (2010) find a similar result using SST anomalies in the Benguela Current. Analyzed by season, the summer rainfall shows the negative signal has a NW orientation consistent with diminished cloud bands. Only the eastern coastal plains (Mozambique) show a positive regression. In the March–May transition season, the negative rain–SST regression persists, and the only positive area is near Cape Town. During winter little rain falls over the interior, but KwaZulu-Natal June–August rainfall shows a negative regression with Agulhas SST. Finally, during the September–November transition season, the expected positive regression between South African rainfall and Agulhas SST emerges to the east of 26°E covering the Drakensberg escarpment (eastern Cape to Swaziland). During spring, much of the rainfall derives from cutoff lows undercut by ridging anticyclones that sweep Agulhas air onto the eastern plateau.

Since most research has underscored an apparent positive influence of the Agulhas Current on South African rainfall anomalies, the statistical analysis is extended to consider vegetation anomalies 1981–2006 (Figure 3f). Again a widespread negative regression is found ($<-0.05°C^{-1}$), particularly in a N–S axis 20°–28°E. Only the coastal fringe shows a positive influence. This unexpected result suggests the Agulhas Current diverts rainfall away from the interior of South Africa. Is the thermal footprint driven by ENSO and more effect than cause?

3.4. Moisture source and sink

The sensitivity of latent heat flux patterns is studied. Regression of the detrended Agulhas SST index onto MERRA LHF anomalies from 1980 to 2012 is mapped over the Agulhas Current and South Africa in Figures 4a–e. The pattern is consistent with GPCC rainfall in that a negative signal is obtained over the interior using year-round anomaly fields. Southwest of Cape Town, and along the south coast, there is a positive influence denoting moisture surplus. Individual seasons mirror the rainfall pattern with positive LHF regression over marine areas in summer and moisture deficits over the interior $< -20\,\mathrm{W\,m^{-2}\,°C^{-1}}$, which intensify in the March–May season. During winter the Agulhas Current becomes a moisture sink and the terrestrial signal weakens. In the spring transition season (September–November), the overall pattern is inverted: positive LHF regression $> +20\,\mathrm{W\,m^{-2}\,°C^{-1}}$ overlies the eastern Cape and hinterland, paired with a deficit over the Agulhas Current. The year-round ENSO–MEI regression onto LHF anomalies at a 2-month lead (Figure 4f) is similar to the Agulhas SST pattern (Figure 4a), albeit at a one-third magnitude. The interior shows a moisture deficit;

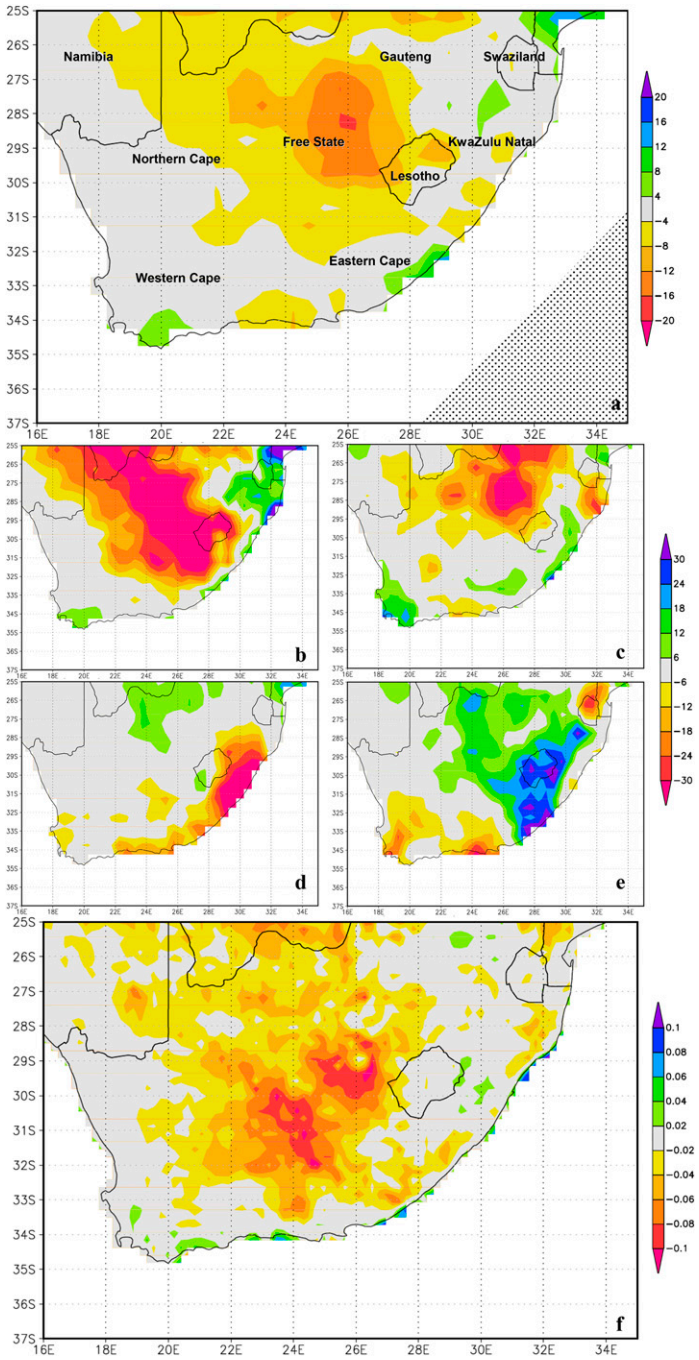

Figure 3. Regression of detrended Agulhas SST anomalies 1950–2012 onto (a) continuous monthly rainfall anomalies; rainfall is shown by season: (b) December–February, (c) March–May, (d) June–August, and (e) September–November. (f) Regression of detrended Agulhas SST onto continuous monthly vegetation fraction anomalies from 1981 to 2006. State labels are given in (a); shaded area refers to lower ship data density. The scale is in mm month^{-1} °C^{-1} in (a)–(e) and the fraction is °C^{-1} in (f).

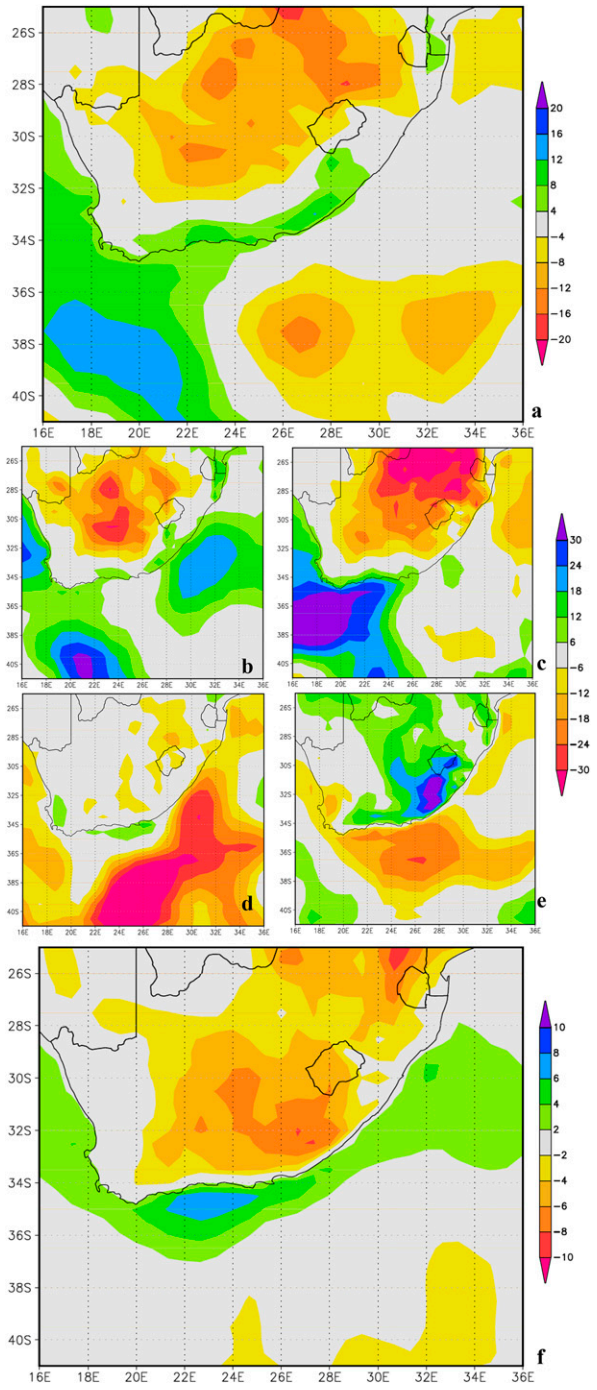

Figure 4. Regression of detrended Agulhas SST anomalies from 1980 to 2012 onto (a) continuous monthly MERRA LHF anomalies; LHF is shown by season: (b) December–February, (c) March–May, (d) June–August, and (e) September–November. The scale in (a) is in units of mm month^{-1} °C^{-1}. (f) Regression of detrended ENSO–MEI onto continuous monthly MERRA LHF anomalies at a 2-month lead; all with units are W m^{-2} °C^{-1}.

only the western Cape shelf exhibits surplus LHF. The ENSO influence on LHF anomalies in the offshore zone is relatively weak.

3.5. Composite analysis

In this section, a composite of 6 cold years is subtracted from 6 warm years to elucidate the processes involved in oceanic warming and continental drying. The upper-ocean analysis (Figure 5a) exhibits westward current differences ($\sim$0.1 m s^{-1}) and a positive salinity signal (about +0.1 ppt) that together indicate a westward extension and acceleration of the south Indian Ocean anticyclonic gyre circulation (Beal et al. 2006), suggesting advective control of SST. In the atmosphere, surface westerly winds increase in the midlatitudes and swerve onto the interior plateau (Figure 5b), advecting dry Benguela air toward a cyclonic vortex at 30°S, 27°E. Despite increased latent heat fluxes in the South Atlantic, there is a negative signal over the western Cape and in the south Indian Ocean. This circulation represents an ''extended winter'' scenario during warm spells in the Agulhas Current, a response consistent with a Pacific El Niño (Hoell et al. 2014). Composite differences in the meridional circulation (Figure 5c) yield the expected moist rising motion over the warmer waters south of South Africa. Upper westerly winds strengthen in the south and weaken in the north, imposing anticyclonic vorticity. The uplifted marine circulation folds into an equatorward flow with a marked sinking component around 500 hPa that extends northward from the Agulhas Current to South Africa's interior plateau. There, the specific humidity exhibits a profound deficit < -4 g kg^{-1}. The overturning atmospheric circulation is the main process by which a warmer Agulhas Current suppresses rainfall over the interior. The equatorward flow opposes the development of NW cloud bands, according to the equation $W = V(\Delta Z)(\beta/f)$, where $f \sim -10^{-4}$ s^{-1} and $\beta = df/dy \sim 10^{-11}$ s^{-1} over 25°–35°S. With an observed $V \sim 5$ m s^{-1} meridional wind and $\Delta Z \sim 5 \times 10^3$ m thickness, a sinking motion W of -2.5×10^{-3} m s^{-1} is estimated. The partial control exerted by the Pacific ENSO on the Agulhas Current makes it a passive responder rather than a driver of multiyear rainfall variability over the interior of South Africa.

4. Conclusions

This study has reconsidered the role of the Agulhas Current in South African climate variability. Expectations were for a positive SST influence on rainfall anomalies over the subcontinent. Here, the Agulhas domain was delimited by the anticyclonic loop of its currents and by cluster analysis of detrended Hadley SST anomalies. This led to an index averaged over an area 28°–37°S, 18°–35°E poleward of South Africa, which excludes the neighboring ocean gyre circulations, the Mozambique Channel, and the Benguela Current. Regressions with GPCC rainfall gave a surprising result of negative influence over the interior. In summer, the negative regression < -20 mm month^{-1} °C^{-1} exhibited a NW axis consistent with reduced cloud band activity. Positive influence was confined to the eastern escarpment in the September–November spring season when cutoff lows are prevalent. The overall negative influence of detrended Agulhas SST anomalies was confirmed by regression with the NASA vegetation fraction and MERRA latent heat flux.

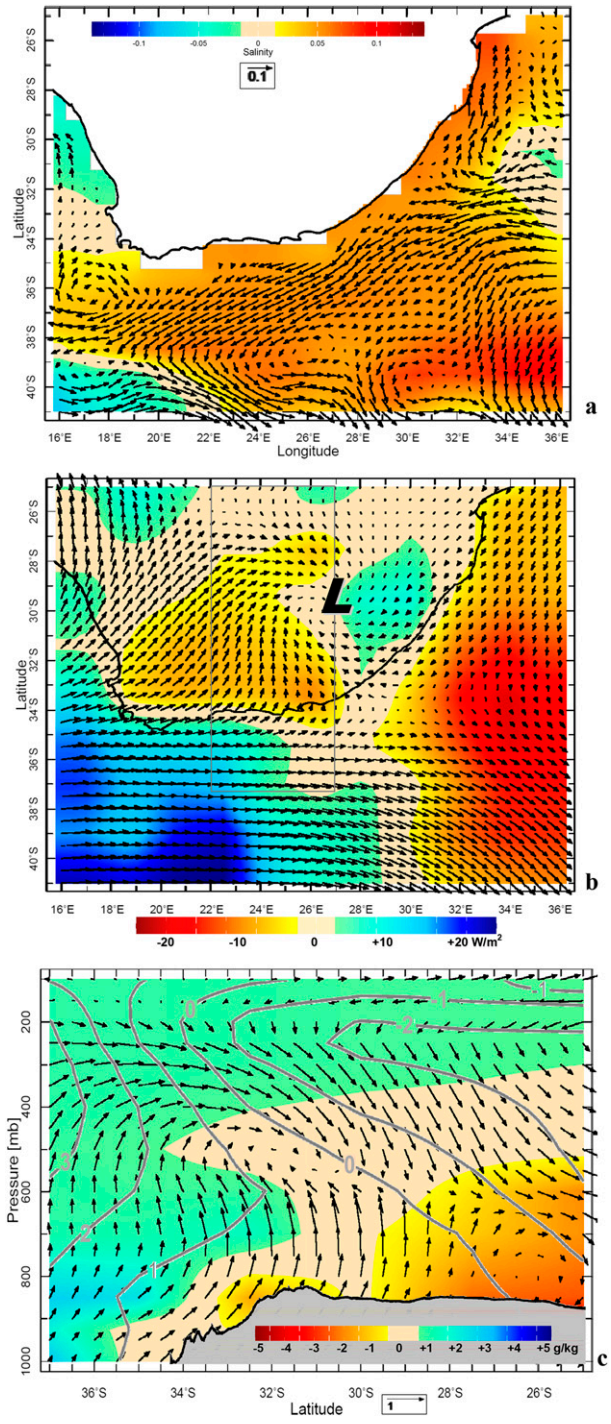

Figure 5. Composite six warm minus six cool Agulhas SST years: (a) 1–100-m ocean salinity and currents, (b) surface wind and latent heat flux with section area, (c) height section averaged 22°–27°E of meridional circulation (vectors), zonal wind (contours), and specific humidity (shading). Cyclonic vortex is highlighted in (b).

Mechanisms of South African rainfall suppression were investigated. The Agulhas SST index was positively related to ENSO–MEI particularly at 1–3-month lead. Hence, warm years in the current south of Africa follow warm El Niño years in the east Pacific. A teleconnection was evident in composite analysis: enhanced westerly winds offshore and an acceleration and westward extension of the anticyclonic loop of salty water from the south Indian Ocean. In this scenario, the warm pool created by the Agulhas Current is more driven by advection than surface flux. The atmospheric composite highlighted that moist air being lifted over a warmer Agulhas Current folds into an equatorward circulation. This causes dry air to sink over the interior plateau, opposing NW cloud bands. The Agulhas Current apparently diverts rainfall away from South Africa except during the spring transition season. Because SST variability in the Agulhas partially follows ENSO, its suppression of interior rainfall is considered to be passive. Further research could include a heat budget analysis to quantify the factors driving SST variability in the Agulhas Current.

Acknowledgments. Useful feedback was received from M. Rouault and C. J. C. Reason of the University of Cape Town. The websites of the IRI Climate Library (for CHIRPS, GODAS, NASA, and NOAA) and Climate Explorer KNMI (for GPCC and MERRA) were used in data extraction, statistical analysis, and graphical mapping. SAPSE funding support from South Africa is acknowledged.

References

Barclay, J. J., M. R. Jury, and W. Landman, 1993: Climatological and structural differences between wet and dry troughs over southern Africa in the early summer. *Meteor. Atmos. Phys.*, **51**, 41–54, doi:10.1007/BF01080879.

Beal, L. M., T. K. Chereskin, Y. D. Lenn, and S. Elipot, 2006: The sources and mixing characteristics of the Agulhas Current. *J. Phys. Oceanogr.*, **36**, 2060–2074, doi:10.1175/JPO2964.1.

Behringer, D. W., 2007: The Global Ocean Data Assimilation System (GODAS) at NCEP. *Proc. 11th Symp. on Integrated Observing and Assimilation Systems for the Atmosphere, Oceans, and Land Surface*, San Antonio, TX, Amer. Meteor. Soc., 3.3. [Available online at https://ams.confex.com/ams/87ANNUAL/webprogram/Paper119541.html.]

Derber, J. C., and A. Rosati, 1989: A global oceanic data assimilation system. *J. Phys. Oceanogr.*, **19**, 1333–1347, doi:10.1175/1520-0485(1989)019<1333:AGODAS>2.0.CO;2.

Fauchereau, N., B. Pohl, C. J. C. Reason, M. Rouault, and Y. Richard, 2009: Recurrent daily OLR patterns in the southern Africa/southwest Indian Ocean region, implications for South African rainfall and teleconnections. *Climate Dyn.*, **32**, 575–591, doi:10.1007/s00382-008-0426-2.

Funk, C. C., and Coauthors, 2014: A quasi-global precipitation time series for drought monitoring. U.S. Geological Survey Data Series 832, 4 pp., doi:10.3133/ds832.

Harrison, M. S. J., 1984: A generalized classification of South African summer rain-bearing synoptic systems. *J. Climatol.*, **4**, 547–560, doi:10.1002/joc.3370040510.

Hart, N. C. G., C. J. C. Reason, and N. Fauchereau, 2013: Cloud bands over southern Africa: Seasonality, contribution to rainfall variability and modulation by the MJO. *Climate Dyn.*, **41**, 1199–1212, doi:10.1007/s00382-012-1589-4.

Hermes, J. C., C. J. C. Reason, and J. R. E. Lutjeharms, 2007: Modeling the variability of the greater Agulhas Current system. *J. Climate*, **20**, 3131–3146, doi:10.1175/JCLI4154.1.

Hoell, A., C. Funk, T. Magadzire, J. Zinke, and G. Husak, 2014: El Niño–Southern Oscillation diversity and southern Africa teleconnections during austral summer. *Climate Dyn.*, **45**, 1583–1599, doi:10.1007/s00382-014-2414-z.

Huang, B., Y. Xue, and D. W. Behringer, 2008: Impacts of Argo salinity in NCEP Global Ocean Data Assimilation System: The tropical Indian Ocean. *J. Geophys. Res.*, **113**, C08002, doi:10.1029/2007JC004388.

Hulme, M., D. Conway, A. M. Joyce, and H. M. Mulenga, 1996: A 1961–90 climatology for Africa south of the equator and a comparison of potential evapotranspiration estimates. *S. Afr. J. Sci.*, **92**, 334–343.

Jimenez, C., and Coauthors, 2011: Global intercomparison of 12 land surface heat flux estimates. *J. Geophys. Res.*, **116**, D02102, doi:10.1029/2010JD014545.

Jury, M. R., H. R. Valentine, and J. R. E. Lutjeharms, 1993: Influence of the Agulhas Current on summer rainfall along the southeast coast of South Africa. *J. Appl. Meteor.*, **32**, 1282–1287, doi:10.1175/1520-0450(1993)032<1282:IOTACO>2.0.CO;2.

——, M. Rouault, S. Weeks, and M. Schormann, 1997: Atmospheric boundary layer fluxes and structure across a land-sea transition zone in southeastern Africa. *Bound.-Layer Meteor.*, **83**, 311–330, doi:10.1023/A:1000295700599.

——, 2002: Economic impacts of climate variability in South Africa and development of resource prediction models. *J. Appl. Meteor.*, **41**, 46–55, doi:10.1175/1520-0450(2002)041<0046:EIOCVI>2.0.CO;2.

Kanamitsu, M., W. Ebisuzaki, J. Woollen, S. K. Yang, J. J. Hnilo, M. Fiorino, and G. L. Potter, 2002: NCEP–DOE AMIP-II Reanalysis (R-2). *Bull. Amer. Meteor. Soc.*, **83**, 1631–1643, doi:10.1175/BAMS-83-11-1631.

Kennedy, J. J., N. A. Rayner, R. O. Smith, M. Saunby, and D. E. Parker, 2011: Reassessing biases and other uncertainties in sea-surface temperature observations since 1850: 1. Measurement and sampling errors. *J. Geophys. Res.*, **116**, D14103, doi:10.1029/2010JD015218.

Mason, S. J., and M. R. Jury, 1997: Climate change and variability over southern Africa: A reflection on underlying processes. *Prog. Phys. Geogr.*, **21**, 23–50, doi:10.1177/030913339702100103.

Matano, R. P., E. J. Beier, P. T. Strub, and R. Tokmakian, 2002: Large-scale forcing of the Agulhas variability: The seasonal cycle. *J. Phys. Oceanogr.*, **32**, 1228–1241, doi:10.1175/1520-0485(2002)032<1228:LSFOTA>2.0.CO;2.

Mo, K., and J. N. Paegle, 2001: The Pacific–South American modes and their downstream effects. *Int. J. Climatol.*, **21**, 1211–1229, doi:10.1002/joc.685.

Nakamura, M., 2012: Impacts of SST anomalies in the Agulhas Current system on the regional climate variability. *J. Climate*, **25**, 1213–1229, doi:10.1175/JCLI-D-11-00088.1.

Reason, C. J. C., 2001: Evidence for the influence of the Agulhas Current on regional atmospheric circulation patterns. *J. Climate*, **14**, 2769–2778, doi:10.1175/1520-0442(2001)014<2769:EFTIOT>2.0.CO;2.

Rienecker, M. M., and Coauthors, 2011: MERRA: NASA's Modern-Era Retrospective Analysis for Research and Applications. *J. Climate*, **24**, 3624–3648, doi:10.1175/JCLI-D-11-00015.1.

Roberts, J. B., F. R. Robertson, C. A. Clayson, and M. G. Bosilovich, 2012: Characterization of turbulent latent and sensible heat flux exchange between the atmosphere and ocean in MERRA. *J. Climate*, **25**, 821–838, doi:10.1175/JCLI-D-11-00029.1.

Rouault, M., S. A. White, C. J. C. Reason, J. R. E. Lutjeharms, and I. Jobard, 2002: Ocean–atmosphere interaction in the Agulhas Current region and a South African extreme weather event. *Wea. Forecasting*, **17**, 655–669, doi:10.1175/1520-0434(2002)017<0655:OAIITA>2.0.CO;2.

——, C. J. C. Reason, J. R. E. Lutjeharms, and A. C. M. Beljaars, 2003: Underestimation of latent and sensible heat fluxes above the Agulhas Current in NCEP and ECMWF analyses. *J. Climate*, **16**, 776–782, doi:10.1175/1520-0442(2003)016<0776:UOLASH>2.0.CO;2.

——, B. Pohl, and P. Penven, 2010: Coastal oceanic climate change and variability from 1982 to 2009 around South Africa. *Afr. J. Mar. Sci.*, **32**, 237–246, doi:10.2989/1814232X.2010.501563.

Schneider, U., A. Becker, P. Finger, A. Meyer-Christoffer, M. Ziese, and B. Rudolf, 2014: GPCC's new land surface precipitation climatology based on quality-controlled in situ data and its role in quantifying the global water cycle. *Theor. Appl. Climatol.*, **115**, 15–40, doi:10.1007/s00704-013-0860-x.

Schulze, R. E., G. A. Kiker, and R. P. Kunz, 1993: Global climate change and agricultural productivity in southern Africa. *Global Environ. Change*, **3**, 330–349, doi:10.1016/0959-3780(93)90022-D.

Tucker, C. J., J. E. Pinzon, M. E. Brown, D. Slayback, E. W. Pak, R. Mahoney, E. Vermote, and N. El Saleous, 2005: An extended AVHRR 8-km NDVI data set compatible with MODIS and SPOT vegetation NDVI data. *Int. J. Remote Sens.*, **26**, 4485–4498, doi:10.1080/01431160500168686.

Walker, N. D., 1990: Links between South African summer rainfall and temperature variability of the Agulhas and Benguela Current systems. *J. Geophys. Res.*, **95**, 3297–3319, doi:10.1029/JC095iC03p03297.

——, and R. D. Mey, 1988: Ocean–atmosphere heat fluxes within the Agulhas retroflection region. *J. Geophys. Res.*, **93**, 15 473–15 483, doi:10.1029/JC093iC12p15473.

Wolter, K., and M. S. Timlin, 2011: El Niño/Southern Oscillation behaviour since 1871 as diagnosed in an extended multivariate ENSO index (MEI.ext). *Int. J. Climatol.*, **31**, 1074–1087, doi:10.1002/joc.2336.